PROCEEDINGS OF SPIE

SPIEDigitalLibrary.org/conference-proceedings-of-spie

Carbon nanotube microfabricated window with extreme ultraviolet transmission and differential pumping

Scott Olsen, Richard Vanfleet, David Allred, Robert Davis

Scott Olsen, Richard Vanfleet, David Allred, Robert Davis, "Carbon nanotube microfabricated window with extreme ultraviolet transmission and differential pumping," Proc. SPIE 12201, UV and Higher Energy Photonics: From Materials to Applications 2022, 1220102 (3 October 2022); doi: 10.1117/12.2631989

SPIE.

Event: SPIE Nanoscience + Engineering, 2022, San Diego, California, United States

Downloaded From: https://www.spiedigitallibrary.org/conference-proceedings-of-spie on 08 Oct 2022 Terms of Use: https://www.spiedigitallibrary.org/terms-of-use

Carbon nanotube microfabricated window with extreme ultraviolet transmission and differential pumping

Scott Olsen, Richard Vanfleet, David Allred, and Robert Davis

Brigham Young University, Provo, Utah

ABSTRACT

Hollow cathode plasmas are common extreme ultraviolet (EUV) lamps used for material characterization. However, the relatively high pressure of the plasma can affect downstream instruments, as well as absorb the EUV. EUV windows are difficult to fabricate due to EUV's strong interaction with all materials. We present a carbon nanotube (CNT) microfabricated window composed of multiple high aspect-ratio columns in parallel. The open areas allow wide bandpass transmission, while the walls restrict gas flow. We model the CNT window transmission as a weight function on the light from of a Mcpherson 629-like hollow cathode helium plasma in visible wavelengths. We model the CNT window differential pumping as a series of columns between two chambers of different pressures.

Keywords: Extreme Ultraviolet, hollow cathode, helium, carbon nanotubes

1. INTRODUCTION

The extreme ultraviolet (EUV) range has much potential in high resolution systems. EUV sources include free electron lasers, synchrotrons, laser-produced plasmas, and discharge-produced plasmas. The latter two are considered common sources and can be broadband or narrowband. Multilayered mirrors are often used in the EUV range; however, their narrow bandwidth can greatly reduce the transmission of broadband sources. To increase transmission, these broadband sources require wide bandpass windows.[1] Many materials are opaque at this and lower wavelength ranges,[2] which makes developing a wide bandpass window difficult. Windowless transitions between chambers have been practiced for hard x-rays for several years. This is also difficult below the VUV range because many applications require a different pressure than the source.[2] In this paper, we present a carbon nanotube (CNT) fabricated window that provides a wide bandpass, high transmission, and differential pumping.

CNTs have much possibility in MEMs applications. At Brigham Young University, we fabricate CNT MEMs devices by patterning a catalyst film onto a substrate, growing the CNTs via CVD, and then filtrating with a filler material via CVD. RIE etching and removal from the substrate leaves a high-aspect ratio structure with the shape and electrical conductivity of the CNTs, but the mechanical properties of the filler material.[3] The structure presented in this paper has demonstrated previously to collimate visible light outside of vacuum.[4]

The column width and wall thickness are determined by catalyst film pattern, while the height is determined by the duration of CNT growth. The structures are infiltrated with carbon to improve stability. The column width and height can be tailored to meet the necessary visible/EUV transmission while providing a pressure ratio between chambers.

2. THEORY

Fig 1 is an image of system used to test the CNT window for light transmission and differential pumping. Modelling the system involves 3 components: determining the intensity distribution of the plasma, the effect of the CNT window on the light transmission through the aperture between the anode and the lower chamber, and the effect of the CNT window on the pressure ratio between the anode and the lower chamber.

UV and Higher Energy Photonics: From Materials to Applications 2022, edited by Yong-Hoon Cho, Gilles Lérondel, Atsushi Taguchi, Proc. of SPIE Vol. 12201, 1220102 · © 2022 SPIE · 0277-786X · doi: 10.1117/12.2631989

Downloaded From: https://www.spiedigitallibrary.org/conference-proceedings-of-spie on 08 Oct 2022
Terms of Use: https://www.spiedigitallibrary.org/terms-of-use

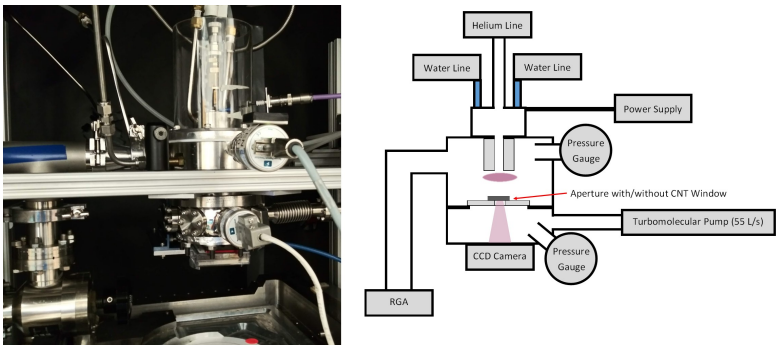


Figure 1. Photograph of experiment (left) and illustration of components (right).

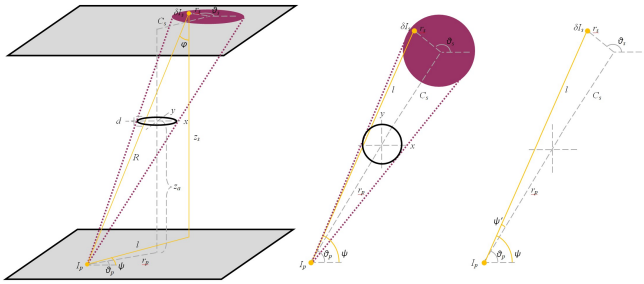


Figure 2. Model of experiment. Far left shows the 3 planes considered: source plane, aperture plane, and observing plane. Middle and far right are viewed along the optical axis. Far right shows the geometry for calculating ψ.

2.1 Plasma Distribution

Fig 2 shows the model for determining the plasma intensity distribution. We state the following assumptions in deriving this model:

- The plasma is a radially symmetric, nonuniform, incoherent intensity distribution[5] at the end of the cathode.
- The hollow cathode and aperture are centered on the optical axis
- Diffraction due to the aperture is negligible

To begin, we consider an infinitismal amount of intensity at a point of interest on the photodiode plane (δI_p) due to the power emitted by a point source ($\delta P_s = I_s(r_s, \theta_s)\delta A$) on the source plane:

$$\delta I_p(r_p, \theta_p) = \frac{I_s(r_s, \theta_s)\delta A}{4\pi R^2} \tag{1}$$

where R is the distance between $I_p(r_p, \theta_p)$ and $I_s(r_s, \theta_s)\delta A$. We then integrate over all the point sources to obtain the total intensity at the point of interest. The integration bounds are then defined by the aperture. Assuming a circular aperture centered on the optical axis that is thin compared to the experiment's overall dimensions, we can find the integration bounds by projecting the aperture onto the source plane from the point of interest. This creates a circle on the source plane with the center located at C_s and radius r_s, which we find to be $r_s(\frac{z_s}{z_a} - 1)$ and $\frac{d}{2}(\frac{z_s}{z_a})$, respectively. Evaluating R, we have:

$$I_p(r_p, \theta_p) = \frac{1}{4\pi} \int_0^{2\pi} \int_0^{\frac{d}{2}(\frac{z_s}{z_a})} \frac{I_s(r_s, \theta_s)}{z_s^2 + r_s^2 + r_p^2(\frac{z_s}{z_a})^2 - 2r_s r_p(\frac{z_s}{z_a})\cos(\theta_s - \theta_p)} r_s \delta r_s \delta\theta_s \tag{2}$$

Further author information:
R. Vanfleet: E-mail: rrv3@byu.edu, Telephone: 801 422 1702

Downloaded From: https://www.spiedigitallibrary.org/conference-proceedings-of-spie on 08 Oct 2022
Terms of Use: https://www.spiedigitallibrary.org/terms-of-use

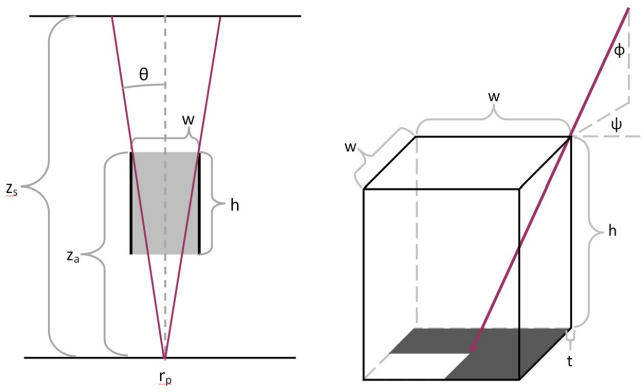


Figure 3. Model for CNT window weight function. The left images shows that the range of angles entering a single column is essentially zero. Because of this, we can equate the loss in intensity to the loss in area (right image).

This requires that we know $I_s(r_s, \theta_s)$, the intensity profile of the plasma. The profile is a function of plasma composition, current, pressure, geometry, and the wavelength being observed.[5] We consider a radially symmetric model involving two Gaussians:

$$I_s(r) = a\left(e^{b(r-c)^2} + e^{b(r+c)^2}\right) \tag{3}$$

where a, b, and c are to be determined experimentally.

2.2 CNT Window

The effect of inserting a CNT window into the system can be modelled using a weight function inside the integral. First, we consider the range of angles that enter a single column in the window (Fig 3). We find that the maximum angle (θ) is equal to $\arctan(w/z_a)$. If $w << z_a$, then the range is approximately zero, meaning that the light entering a single column is essentially collimated. Following Westover,[4] we can then consider the amount of open area at a given incident angle (ϕ) as proportional to the amount of intensity exiting the column. Taking into account an azimuthal angle ψ, we have the area equal to $(w - \tan\phi\cos\psi)(w - \tan\phi\sin\psi)$. The weight function is then:

$$C = \frac{I(\phi, \psi, w, h)}{I_0} = \frac{(w - h\tan\phi\cos\psi)(w - h\tan\phi\sin\psi)}{(w+t)^2} \tag{4}$$

Note that this reduces to an equation similar to that given by Westover when $\psi = 0$, as we expect. However, it also needs to reduce that equation when $\psi = \pi/2$, π, and $3\pi/2$. This requires to take the absolute values of the $\cos\psi$ and $\sin\psi$ terms. We also need to consider the collimating angle ϕ_c, beyond which no intensity makes it through the column. To do determine ϕ_c, we set $C = 0$ and solve. To make $C = 0$ beyond ϕ_c, we use heaviside functions:

$$C = \frac{(w - h|\tan\phi\cos\psi|)(w - h|\tan\phi\sin\psi|)}{(w+t)^2}\Theta\left(\frac{w}{h|\cos\psi|} - |\tan\phi|\right)\Theta\left(\frac{w}{h|\sin\psi|} - |\tan\phi|\right) \tag{5}$$

The final step is to write ϕ and ψ in terms of the variables already introduced. for which we refer back to Fig 2. We see that $\tan\phi = l/z_s$, where $l = \sqrt{r_p^2(\frac{z_s}{z_a})^2 + r_s^2 - 2r_s r_p(\frac{z_s}{z_a})\cos(\theta_s - \theta_p)}$. ψ depends on how r_s compares to r_p and θ_s to θ_p. For the condition shown in Fig 2, we find that $\psi = \theta_p + \psi'$, where ψ' is evaluated using the law of cosines. Solving for ψ for all possible conditions, we summarize the results in Table 1.

2.3 Differential Pumping

The restriction on gas flow is modelled by calculating the conductance of the CNT window mounted to an aperture. We begin by calculating the conductance of a single column. Assuming molecular flow regime, the

Downloaded From: https://www.spiedigitallibrary.org/conference-proceedings-of-spie on 08 Oct 2022
Terms of Use: https://www.spiedigitallibrary.org/terms-of-use

Condition 1	ψ'	Condition 2	ψ
$r_s < r_p(\frac{z_s}{z_a})$	$\psi' = \arccos \frac{r_p^2(\frac{z_s}{z_a})^2 + l^2 - r_s^2}{2lr_p(\frac{z_s}{z_a})}$	$\theta_p - \pi < \theta_s < \theta_p$ $\theta_p < \theta_s < \theta_p + \pi$	$\psi = \theta_p + \psi'$ $\psi = \theta_p - \psi'$
$r_s > r_p(\frac{z_s}{z_a})$	$\psi' = \arccos \frac{r_s^2 + l^2 - r_p^2(\frac{z_s}{z_a})^2}{2lr_s}$	$\theta_s - \pi < \theta_p < \theta_s$ $\theta_s < \theta_p < \theta_s + \pi$	$\psi = \theta_s - \psi'$ $\psi = \theta_s + \psi'$

Table 1. Conditions for determining *psi*, then azimuthal angle at which light enters a column.

conductance of the opening and length of the column are given in L/s by Eq 6 and 7, respectively.

$$C_{opening} = 3.64w^2\sqrt{\frac{T}{M}} \tag{6}$$

$$C_{pipe} = 9.70\frac{w^3}{2h}\sqrt{\frac{T}{M}} \tag{7}$$

where T is temperature in Kelvin, M is the molecular weight of the gas in kg/mol, h and w are the height and width of the column in cm, respectively.[6] Adding the two conductances in series gives the conductance of one column:

$$C_{column} = \frac{1}{\frac{1}{C_{opening}} + \frac{1}{C_{pipe}}} \tag{8}$$

Then multiply by the number of columns to obtain the conductance of a structure with area A:

$$C_{window} = N_{columns}C_{column} \approx \frac{A}{A_{column}}C_{column} = \frac{AC_{column}}{(w+t)^2} \tag{9}$$

Assuming the thickness of the walls (t) is much less than the pore size (w), the conductance is approximately:

$$C_{window} \approx \frac{AC_{column}}{w^2} = \frac{A}{0.275 + 0.206\frac{h}{w}}\sqrt{\frac{T}{M}} \tag{10}$$

This conductance must be added in series to the conductance of the aperture, $C_{aperture}$, which is to be determined experimentally. The pressure ratio is equal to the conductance divided by the pumping speed of the pump connected to the lower pressure chamber. Therefore, the expected pressure ratio of the CNT collimator mounted to an aperture is given by:

$$\frac{P_L}{P_H - P_L} = \frac{1}{S} * \frac{A}{(0.275 + 0.206\frac{h}{w})\sqrt{\frac{M}{T}} + \frac{A}{C_{aperture}}} \tag{11}$$

Where S is the pumping speed in L/s, A is in cm2, and P_L and P_H are the low and high pressures in torr, respectively.[6]

3. FABRICATION

Preparation of the substrate and CNT growth are outlined in.[4] CNT growth was done at 750 C with 311 sccm of hydrogen and 338 sccm of ethylene for 30 minutes. Carbon infiltration was done at 900 C with 311 sccm of hydrogen and 338 sccm of ethylene for 4-5 minutes. Once removed from the furnace, the CNT windows were put into a heated 45% KOH bath till the die separated from the windows. The windows were then placed in a water bath, then rinsed with IPA. When dried, they were plasma etched (Technics Planar Etch 2) at about 100 mtorr, 200 W for 2-5 minutes to remove the carbon floor layer. The CNT windows were then mounted to a shim steel aperture about 2 mm in diameter using carbon tape.

Downloaded From: https://www.spiedigitallibrary.org/conference-proceedings-of-spie on 08 Oct 2022
Terms of Use: https://www.spiedigitallibrary.org/terms-of-use

4. EXPERIMENT

We used a helium plasma with a geometry similar to a Mcpherson 629 hollow cathode. The anode was connected to a roughing pump, a turbomolecular pump, a residual gas analyzer (RGA), and a micropirani pressure gauge. At the base of the anode a 3 mm deep well was machined for placement of the shim steel aperture. Under the anode a Kimball spherical octagon vacuum chamber was connected with a viewport facing the aperture, a micropirani gauge, a turbomolecular pump, and a roughing pump.

Alignment of the shim steel aperture involved removing the octagon chamber and inserting a LED light into the cathode bore. The light emanating from the bore was traced at two distances from the cathode. The centers of the circles traced then defined the optical axis. The aperture was then inserted and adjusted to align with the optical axis, then the LED removed.

If a CNT window was mounted to the aperture, then an additional step involved shining a red laser pointer into the anode and through the window. After aligning the laser with the optical axis, the window was tilted till the interference pattern observed was symmetric.

Once the vacuum was closed, the system was pumped down for about 30 minutes. A mass spectrum was taken with the RGA and a leak test conducted using an argon spray gun. The system was then purged with helium at 2.5 torr for 1 hour. After the purge, a plasma was ignited using a high DC voltage power supply. Pressure and current were adjusted to desired values and allowed to settle for 5 minutes.

At each pressure and current considered, 10 images were taken using a ThorLab 1.6 MP CMOS compact scientific camera placed under the viewport. 10 images were also taken after the plasma was extinguished for background noise. For visible trials, a neutral density filter were placed over the camera. For EUV trials, a phosphor screen composed of P43 and 95.6 nm of aluminum was placed over the viewport in vacuum. The images were averaged and the averaged background subtracted. The distribution was then fit to a Gaussian profile along the x and y axes. A Matlab program then calculated I_p at various points using Eq 2 and Eq 3 (Eq 3 multiplied by Eq 5 in case of a CNT window present).

For differential pumping, 18 data points over the course of 5 minutes were taken in the anode and the octagon chamber at various plasma pressures. The points were averaged and the conductance calculated. In the case of no CNT window present, a curve was fitted to the data to determine the shim steel aperture conductance as a function of plasma pressure.

5. DATA AND DISCUSSION

5.1 Plasma Distribution

Three trials were conducted with a $d = 2.154$ mm shim steel aperture and no CNT window present to image the plasma at various pressures and currents in the visible. It was found that b of Eq 3 varied slightly with pressure and current, while c remained constant at 0. A function of current and pressure was fitted to b, given in Eq 12. Using the function's values, the optimal a values were found and a function of current and pressure fitted, (Eq 13). Eq 3, 12, and 13 then establish a model of the intensity distribution for the plasma at various currents and pressures in the visible. Error between the model and data was calculated by summing the standard deviations of fitting the Gaussians to the x and y axes of the image, the standard deviation of averaging the Gaussians' peak, and the root mean square error (RMSE) of the Matlab program to the Gaussian in quadrature, then taking the square root and dividing by the averaged peak. Results are listed in Table 2. Sources of error include misalignment in the aperture, the aperture not being perfectly circular, and surface defects in the viewport.

$$b = (10.65 + 0.9397I + 6.031P) * 10^5 \tag{12}$$

$$a = (0.03433 + 4.74I + 3.859P - 0.7473IP - 3.025P^2) * 10^6 \tag{13}$$

Downloaded From: https://www.spiedigitallibrary.org/conference-proceedings-of-spie on 08 Oct 2022
Terms of Use: https://www.spiedigitallibrary.org/terms-of-use

Trial	I (A)	P_H (torr)	P_L (torr)	I_p Error (%)	$C_{aperture}$ Error (%)
1	1.00	1.04	0.20	3.18	5.54
	0.75	1.03	0.20	2.97	3.55
	0.50	1.00	0.20	2.84	2.28
	0.27	0.96	0.20	3.16	9.00
	1.00	0.76	0.12	3.78	10.67
	1.00	0.52	0.07	3.88	15.48
	1.00	0.28	0.04	3.77	3.60
2	0.76	0.77	0.13	2.51	2.83
	0.51	0.74	0.13	2.68	3.88
	0.27	0.72	0.13	2.96	8.21
	0.75	0.53	0.08	2.89	1.60
	0.75	0.27	0.03	3.11	11.11
3	0.51	0.52	0.08	2.52	1.20
	0.29	0.50	0.08	2.43	6.70
	0.51	0.27	0.04	2.81	7.96

Table 2. Trials conducted without a CNT window present. Between each trial, the vacuum was broken, anode cleaned, and aperture realigned.

5.2 CNT Window

A $w = 50$ microns, $h \approx 850$ microns CNT window was mounted to the aperture and the intensity distribution observed for various plasma pressure and current values, listed in Table 3. Fig 4 shows the Matlab program comparison of the distribution along the axis as observed by the CCD camera due to a $I \approx 0.76$ A, $P \approx 0.53$ torr plasma without a CNT window present (Trial 2-4 in Table 2), the predicted distribution, the distribution with a CNT window present (Trial 1-2 in Table 3), and the predicted distribution.

Trial	I (A)	P_H (torr)	P_L (torr)	I_p Error (%)	$P_L/(P_H - P_L)$ Error (%)
1	0.97	0.53	0.02	8.67	2.39
	0.76	0.54	0.02	8.51	1.32
	0.51	0.58	0.02	8.69	8.08

Table 3. Trial with a CNT window present. Prior to the trial the aperture was aligned using an LED in the anode, then the CNT window was tilted using a laser pointer aligned with the optical axis.

Downloaded From: https://www.spiedigitallibrary.org/conference-proceedings-of-spie on 08 Oct 2022
Terms of Use: https://www.spiedigitallibrary.org/terms-of-use

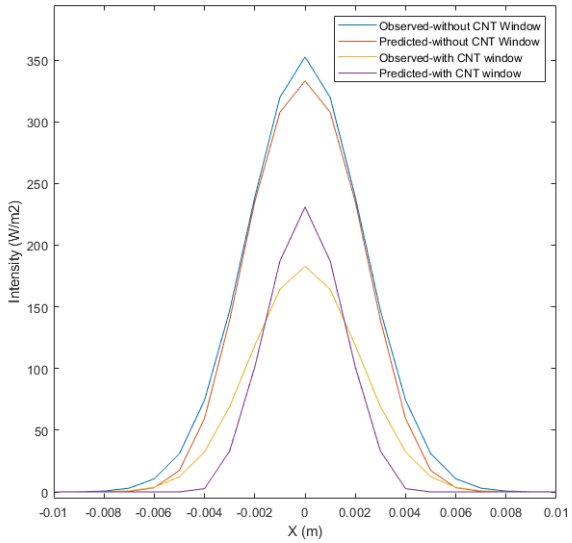


Figure 4. Intensity distributions along the axis as observed by the CCD camera of 1) an observed 0.76 A, 0.53 torr plasma, 2) the predicted of the former, 3) the observed of the same with a CNT window present, and 4) the predicted of the former.

The observed distribution of the CNT window is lower and wider than anticipated. We took into account diffraction by performing a convolution on I_p with the diffraction pattern of a single column, assuming far-field condition, normalized by the integral over the area. This was found to change the errors (in order descending) to 6.75, 8.46, and 8.98%. Other sources of error include height variation along the CNT window, residual tilt of the window, and possible side-wall reflection inside the columns of the window.

5.3 Differential Pumping

Table 2 lists the observed pressures of the plasma (P_H) and the octagon chamber underneath (P_L). The conductance of the aperture was calculated, using $S = 55$ L/s for the turbomolecular pump, and fitted to a function of plasma pressure. The error listed in Table 2 was calculated by summing the standard deviation of P_H, the standard deviation of P_L, and the difference between the predicted value and the observed value in quadrature, then taking the square root and dividing by the observed value. We note that the error in some trials is relatively high (maximum being 15.48%). This may be due to the pumping speed S being a function of pressure- higher pressures may have caused the pump to operate at a lower pumping speed.

Table 3 lists P_H, P_L, and the error between the observed pressure ratio and that predicted by the aperture with the CNT window present us Eq 11. We obtain a pressure ratio of about 0.04 for all runs, which is fairly close to that observed. Sources of error include variable pumping speed, improper mounting of the aperture, height variation along the CNT window, and leaks between the CNT window and the aperture.

6. CONCLUSION

We modelled a Mcpherson 629-like hollow cathode helium plasma in the visible as a function of current and pressure up to 1.00 A and 1.00 torr with an error less than 3.9% of the peak intensity. We have developed a CNT window with high visible transmission and differential pumping. Our model of the CNT window predicts a transmitted distribution with an error less than 8.7% of the peak intensity, and a pressure ratio with an error less than 8.1%. We look forward to modelling the helium plasma in the EUV and the CNT window's EUV transmission.

Downloaded From: https://www.spiedigitallibrary.org/conference-proceedings-of-spie on 08 Oct 2022
Terms of Use: https://www.spiedigitallibrary.org/terms-of-use

ACKNOWLEDGMENTS

We thank BYU's Physics and Astronomy Department, the BYU Graduate Studies HIDRA Fellowship, and Utah NASA Space Grant Consortium (Grant #NNX15AI24H) for funding; John Ellsworth and the BYU Physics Machine Shop for designing and fabricating necessary components; BYU IMF and BYU Microscopy Department for facilities to fabricate and image the CNT windows.

REFERENCES

[1] A. Zameshien, e. a., "Angular and spectral bandwidth of extreme uv multilayered near spacer material absorption edges," *Journal of Nanoscience and Nanotechnology* **19**, 602–608 (2019).

[2] A. Giuliani, e. a., "A differential pumping system to deliver windowless vuv photons at atmospheric pressure," *JOurnal of Synchrotron Radiation* **18**, 546–549 (2011).

[3] D. Hutchison, e. a., "Carbon nanotubes as a framework for high-aspect-ratio mems fabrication," *Journal of Microelectromechanical Systems* **19**, 75–82 (2010).

[4] T. Westover, e. a., "Visible and short-wavelength infrared light collimation through carbon nanotube, parallel-hole collimators," *Optics Express* **30**, 22679–22686 (2022).

[5] Pillow, M., "A critical review of spectral and related physical properties of the hollow cathode discharge," *Spectrochemica Acta* **36(B)**, 821–843 (1981).

[6] Ohring, M., [*Materials Science of Thin Films*], Academic Press (2002).

Downloaded From: https://www.spiedigitallibrary.org/conference-proceedings-of-spie on 08 Oct 2022
Terms of Use: https://www.spiedigitallibrary.org/terms-of-use